Chapter 7

Characterization of boron-doped carbon nanotube arrays

7.1. Introduction

The idea of doping CNTs has been attractive since it allows controlling their electronic properties (by reaction of intercalation with electron donors or acceptors). Boron-doped CNTs are predicted to act as semiconductors among large range diameters and chiralities. Boron-doped CNTs (B/C ratio < 0.05) were reported as by-products when BC_2N CNTs were prepared by an arc-discharge method [1]. In Chapter 5, we have successfully synthesized boron-doped diamond-like emitters in microwave plasma chemical vapor deposition (MPCVD) [2].

In this chapter, boron -doped CNT films were directly synthesized by using trimethylborate $B(OCH_3)_3$ as the same doping sources. CNT films grown on patterned substrate show higher field emission characteristics because of eliminating the shield effect. Boron are expected to dominate the electrical transport of CNT films with improve their electrical property. The possibility to operate CNT devices at high current is thought to be an efficient strategy on the industry application.

7.2. Experiment

Starting substrates were mirror-polish n-type, (100) oriented Si wafer with a resistivity of 4.5~5.5 Ω/cm. Wafers were cleaned by Radio Corporation of America

(RCA) cleaning process to remove contamination on the silicon surface. After cleaning, a SiO_2 dielectric layer was deposited using high temperature and low pressure furnace deposition system (model ASM LB-45). A pattern of 8 μm wide dots with 8 μm space between them was successfully fabricated onto a photoresist layer using ASM PAS 2500/10 G-Line exposer and the Convac CPP-70 developing system. A 150 nm thick film of Fe catalyst was deposited on SiO_2 by using dual E-Gun Evaporator (model ULVAC EBX-10C, Japan). Then, the photoresist was removed by lift-off process in an acetone solution in an ultrasonic agitator. Finally, the patterned substrates were put in microwave plasma chemical vapor deposition (MPCVD) to grow selective patterned deposition (SAD) of CNTs. The reactive gases used in deposition were CH_4-H_2 with flow rate of 10/40 sccm and trimethylborate $B(OCH_3)_3$ as doping source with 0.5; 1 and 2 sccm, respectively. The following table lists the experimental conditions.

Table 7.1 Deposition conditions of undoped and boron-doped carbon nanotubes

Sample	flow rate CH_4/H_2+ doping source (sccm)
A (Undoped)	10/40
B (Boron-doped)	10/40+0.5
C (Boron-doped)	10/40+1
D (Boron-doped)	10/40+2

Deposition time = 10 min
MW power = 400 W
Doping source: $B(OCH_3)_3$

Total pressure =15 torr
Substrate temp. (℃) = ~700

After deposition, the produced CNTs were characterized by scanning electron microscope to observe the length and the morphology. A transmission electron microscope was used to determine the nanostructure of individual CNT. The specimens for transmission electron microscope (TEM) were prepared by dispersing the CNTs with acetone in an ultrasonic bath. A drop of suspension was placed onto a carbon film supported by a Cu grid. A Raman spectrum was used to evaluate the crystallinity. A secondary ion mass spectrometry was used to detect the amount of boron. An I-V measuring system was used to obtain the field emission property.

7.3. Results and Discussion

(I) Scanning electron microscope (SEM)

Figure 7.1 (a)~(c) clearly illustrate well-aligned CNTs can be grown by using Fe catalyst as compared to the previous chapter (using Pd as catalyst). The alignment is maybe resulted from following two reasons. First, the electrical self-bias field imposed on the substrate surface under plasma condition primarily induces the alignment. These electrostatic forces perpendicular to the surface would cause CNTs to maintain the one-dimensional growth direction. This implies that the CNTs' most favorable orientation is affected by the electrostatic align with the field direction. Second, Merkulov et al. [3] has proposed the crowding effect instead of the electrostatic filed force. This suggests that the tensile or compress stress will exist

between nanoparticles and neighboring CNTs. Under nanouniform stress (part tensile, part compressive) generated on the CNTs, the growing direction would be kept on approximately tubular orientation. However, under same experimental condition (including reactive gases, microwave power, working pressure), the CNTs grown on Pd substrate does not exhibit the aligned property. This may be arising from different catalyst effect.

It is worth emphasizing the Fig. 7.2 that denser CNTs not only grow on the Fe substrate but also on the backside, which is catalyst-free. The edge of the backside generates denser CNTs than the center of backside does. Actually, the amount of CNTs on the backside decreases away from the edge. We speculate two possible explains about this phenomenon. First, this may be resulted from the carbon by-products on the holder after previous experiment. It is usually found that the holder would be deposited some carbon materials after experiment. As synthesizing the CNTs, the backside of substrate facing the carbon materials will be adsorbed the carbon species coming from the bombarding carbon materials under local plasma condition. This is similar to the sputtering effect. The other reason may be as a result of over-growing. Due to the catalytic effect, the CNTs are produced drastically on Fe substrate. Thus, the overgrowing CNTs would be extended-distribution from the front to the backside of the substrate.

(a)

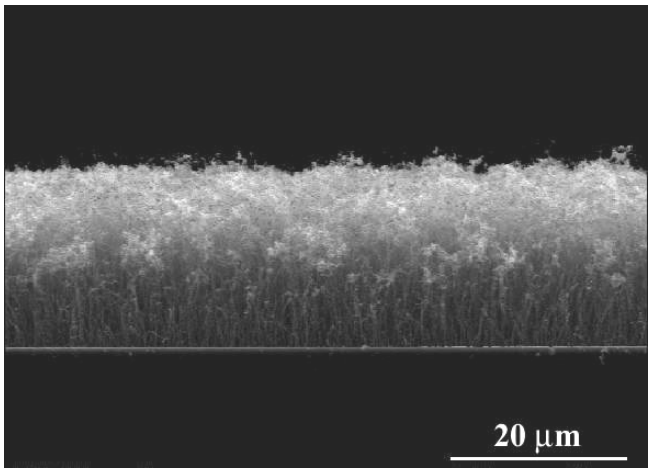

(b)

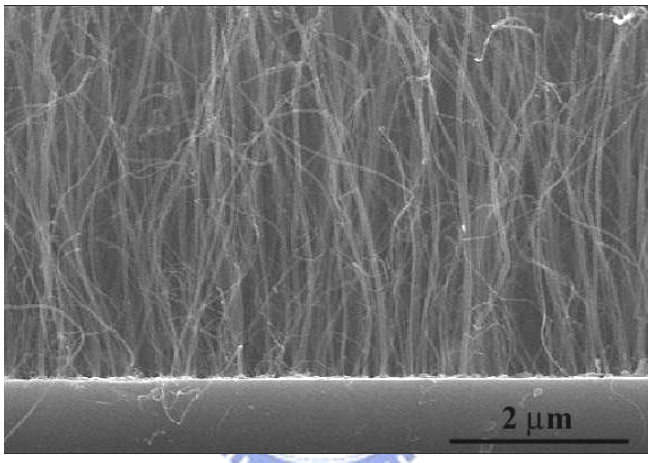

(c)

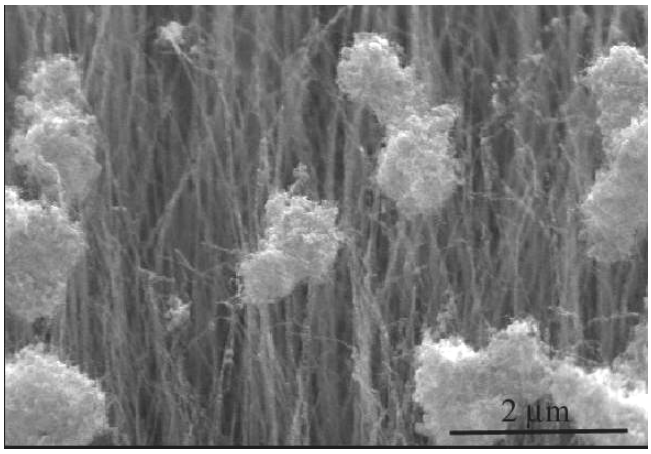

Fig. 7.1 SEM photographs of undoped CNT film (a) cross-section view, (b) low magnification and (c) high magnification view.

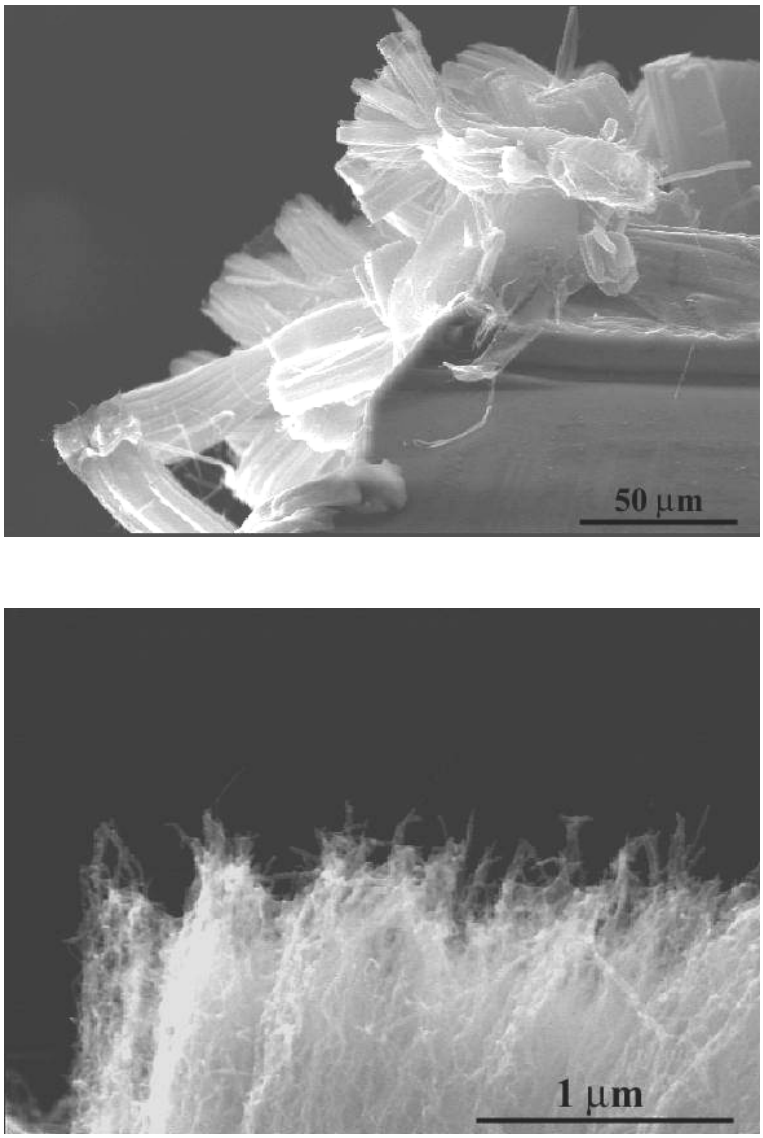

Fig. 7.2 SEM photographs of undoped-CNT films grown on the backside of substrate.

This is why we observe denser CNTs in the edge of backside than in the center position of backside.

As used Fe catalyst, it is also found the coiled CNTs grown on the substrate. Fig. 7.3 display coiled CNTs with various tight angles. The structural model for coiled CNTs is resulted from regular incorporation of pentagon – heptagon pairs in the hexagonal network [4-5]. These defect-based structures of carbon nanotubes are usually found in low growth temperature condition. Under this condition, carbon atoms and clusters have low mobility, which may enhance the quenching of the pentagonal and heptagonal rings in the growing structure. When a stable Haeckelite [6] nucleus is formed, this will continue to grow as a coiled CNTs. It is possible to generate the other structure if the pentagonal and heptagonal rings are taken as regular buildings instead of defects. Recent theoretical calculations showed that one may construct only from pentagons and heptagons “selfcoiling” structures, i.e., structures in which the bond strain is best relaxed when it takes the shape of a torus [7].

Fig. 7.4 (a) and (b) show SEM pictures of undoped and boron-doped CNT arrays, respectively. The photograph on the right side of each figure is an enlarged image. 8 μm-bound aligned CNTs are successfully completed through selective area deposition method. Obviously, it is found that the undoped CNTs possess longer length. Under the SEM analysis, we find that undoped CNTs are denser than boron-doped ones.

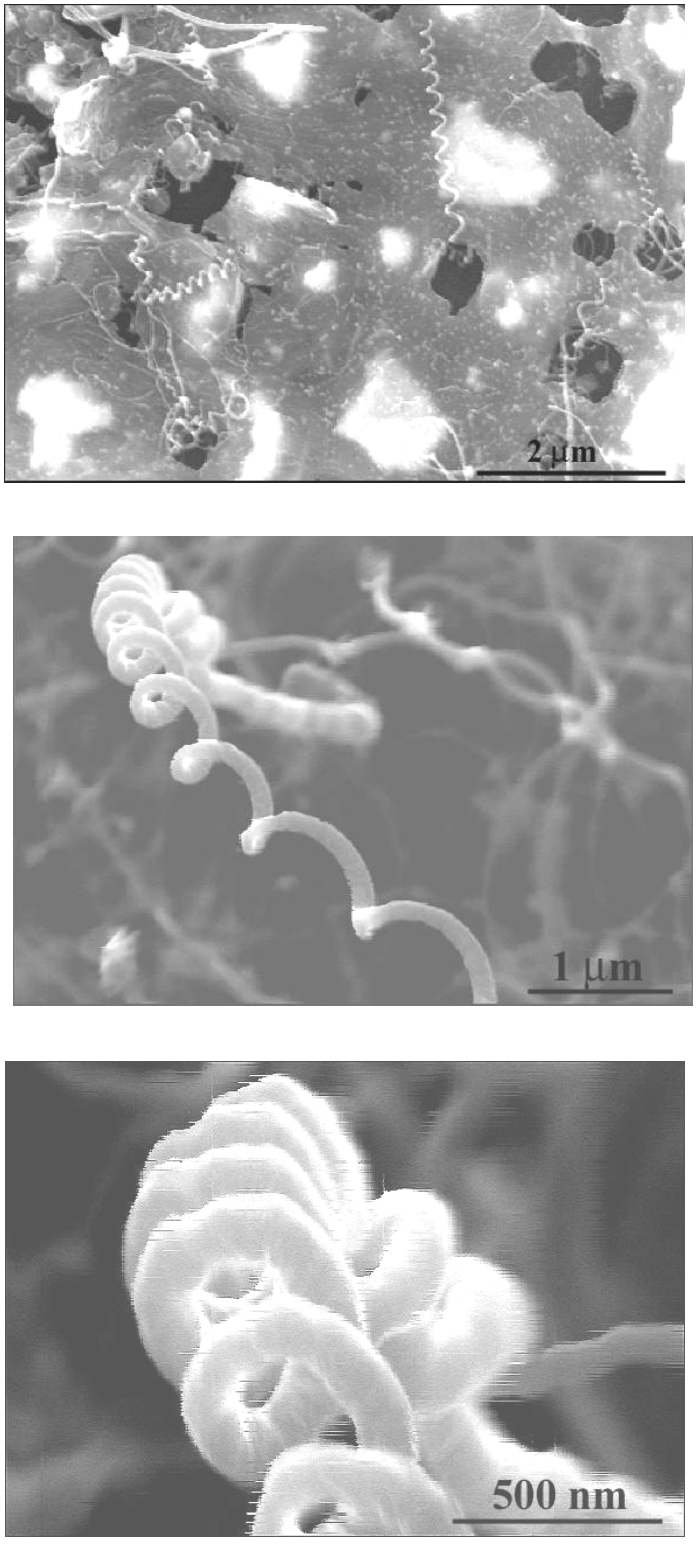

Fig. 7.3 SEM photographs of coiled carbon nanotubes.

(a)

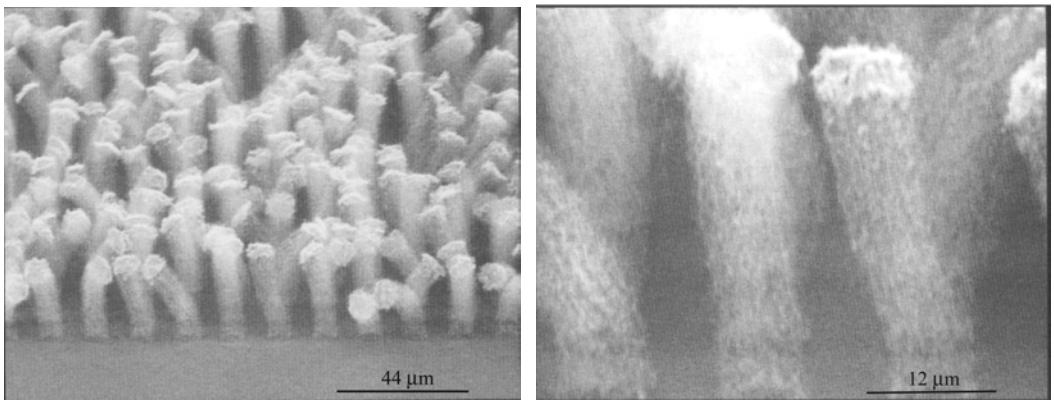

(b)

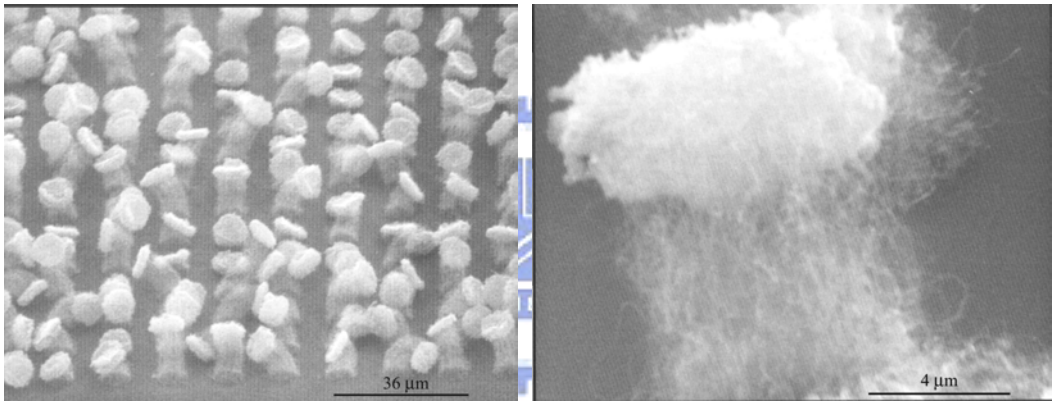

Fig. 7.4 SEM photographs of (a) undoped and (b) boron-doped CNTs arrays.

Comparison between the undoped and boron-doped CNTs shows that the growth rate of undoped CNTs is higher than boron-doped ones. This could be explained by the high oxygen content contained in the $B(OCH_3)_3$. High concentration of oxygen increases the etching rate during CNTs growth. This is in accordance with our previous study where the growth of diamond was inhibited when O_2 was added to the CH_4-CO_2 gas mixture [8]. By using infrared spectroscopy (IR), there is no obvious peak of C-B bonding. In the case of boron dopants, the intercalation of boron is thought to act as dopants in graphite, in between the graphitic shells leading to an internal strain in the interlayer distances. This internal strain resulted from boron would result in expansion and influence the C-C bonding in graphite structure, leading to defects on CNTs. As comparing the alignment of CNTs grown on substrate shown in Fig. 7.1, CNTs grown on patterned substrates tend to exhibit curve orientation. Hence, it is obvious that alignment of CNTs is attributed to the crowing effect, not the plasma-induced effect. In some cases, the crowing effect is usually referred to Van der walls effect.

(II) Transmission electron microscope (TEM)

Figures 7.5 and 7.6 show TEM images of undoped and boron-doped CNTs, respectively. In Fig.7.6, the right side pictures are enlarged images of the ones on the left.

(a)

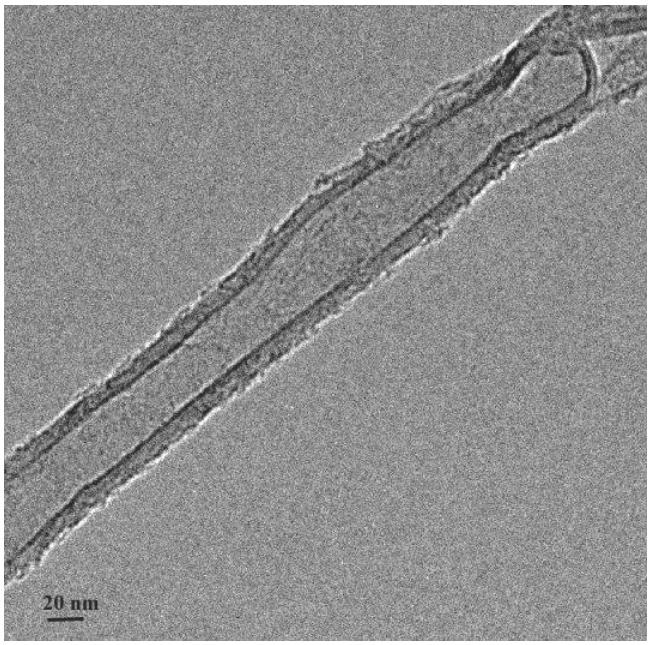

(b)

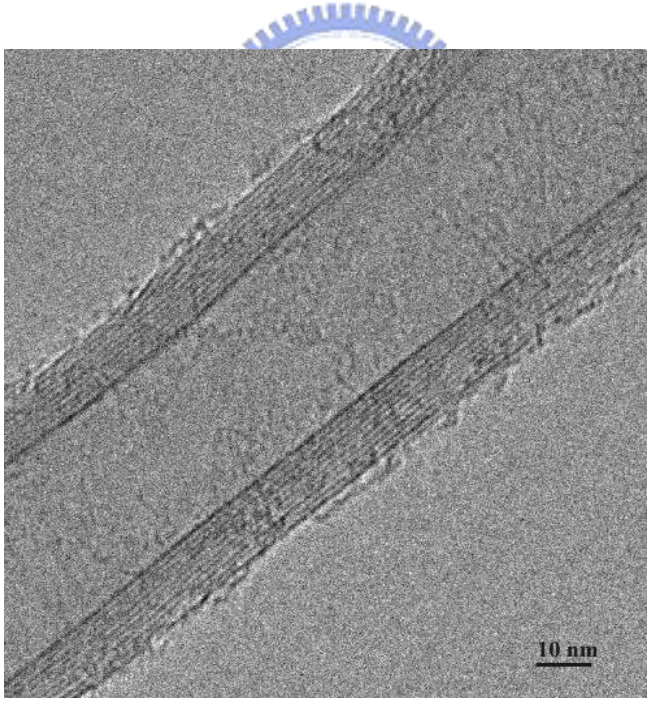

Fig. 7.5 TEM images of undoped CNTs.

(a) $B(OCH_3)_3$= 1 sccm

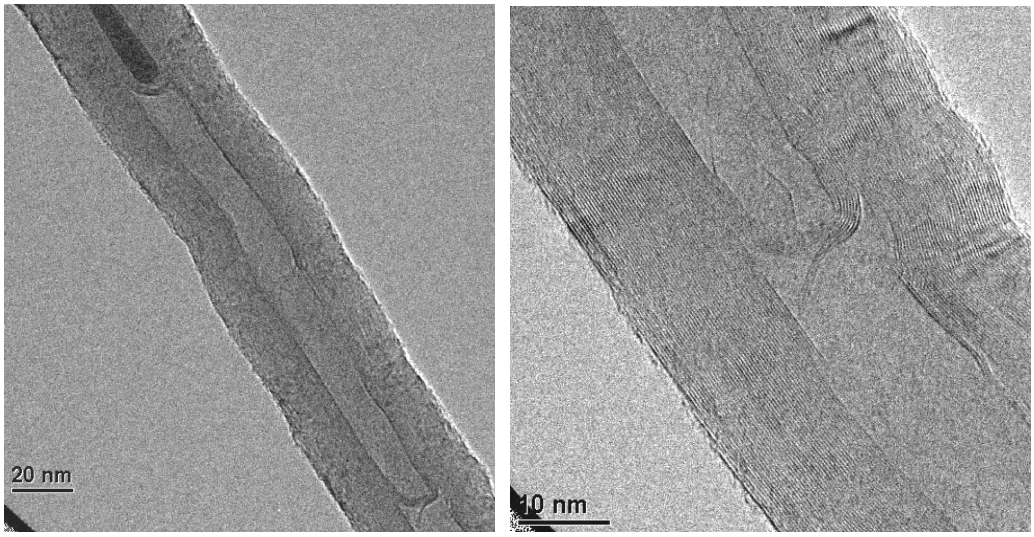

(b) $B(OCH_3)_3$= 2 sccm

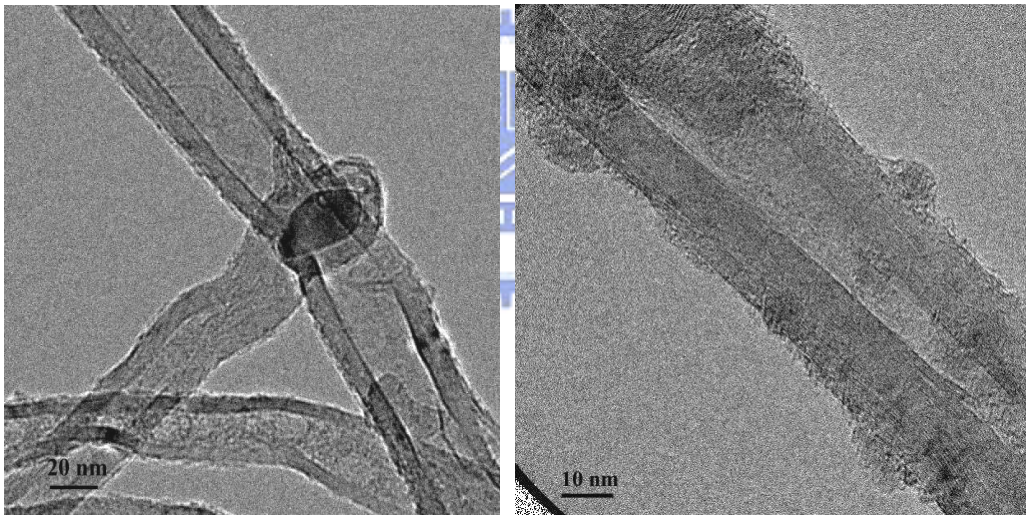

Fig. 7.6 TEM images of boron-doped CNT with various boron concentration at (a) 1 sccm and (b) 2 sccm.

Based on TEM images, the diameter of undoped and boron-doped CNTs are about 50 and 40 nm, respectively. This indicates that boron-doped CNTs have smaller diameter than undoped ones. Compared to the length between undoped and boron-doped CNTs shown in Fig. 1, the difference on diameter is not obvious. As mentioned in SEM section, the expansion in graphitic interlayer and the lower growth rate in boron-doped CNTs simultaneously compete during growth, causing the variation of diameter is not distinguishable. It is found that undoped CNTs are bamboo-like shape. This shape has been reported in many studies as the Fe catalyst is used [9-11]. However, the nanostructured of bamboo-like shape becomes obscure in boron-doped CNTs. As the boron concentration is below 1 sccm, TEM images show slightly distortion and defects on graphite structure. Once increasing the concentration of boron to 2 sccm, the bamboo structure disappears. In addition, Fig. 7.6 (b) also shows that doping source reached to 2 sccm results in much amount of amorphous carbon and structure defect on the CNTs.

(III) Raman spectrum

The first-order Raman spectra of CNTs are shown in Fig. 7.7. The 1580 cm^{-1} band corresponds to one of the two E_{2g} modes assigned to the movement of two neighboring carbon atoms in opposite directions in a graphite sheet [12]. The 1350 cm^{-1} band is normally explained by relaxation of the wave vector selection rule

resulting from the effect of the finite size of crystal in the materials [13]. Boron-doped CNTs also obviously possess these two peaks in spite of the existence of much amount amorphous carbon as mentioned in TEM results. The other conspicuous phenomenon is that the intensity of D line (I_D), meaning disordered graphite increases with increasing concentration of boron. Normally, the I_D / I_G ratio increases with (i) increasing the amount of amorphous carbon in the material and (ii) decreasing the graphite crystal size. Fig. 7.8 indicates the I_D / I_G ratio increases from 0.68 in undoped CNTs to 0.96 when the boron concentration reaches 2 sccm. This implies that doping boron decreases the graphitization. Thus, the boron-doping effect strongly influences the crystallinity of CNTs. This result is also consistent with the previous TEM images.

(IV) Secondary ion mass spectrometry (SIMS)

In this chapter, SIMS is used to detect the surface composition of CNTs. Figure 7.9 displays the depth profile of boron-doped CNTs. The primary beam is O_2 with 8 keV and 140 nA. The detecting rafter areas are set at 225 X 225 μm^2. Based on SIMS results exhibited in Fig. 7.9, there are boron existing in the emitters clearly. It is worth noting that the SIMS detection is only qualitative analysis.

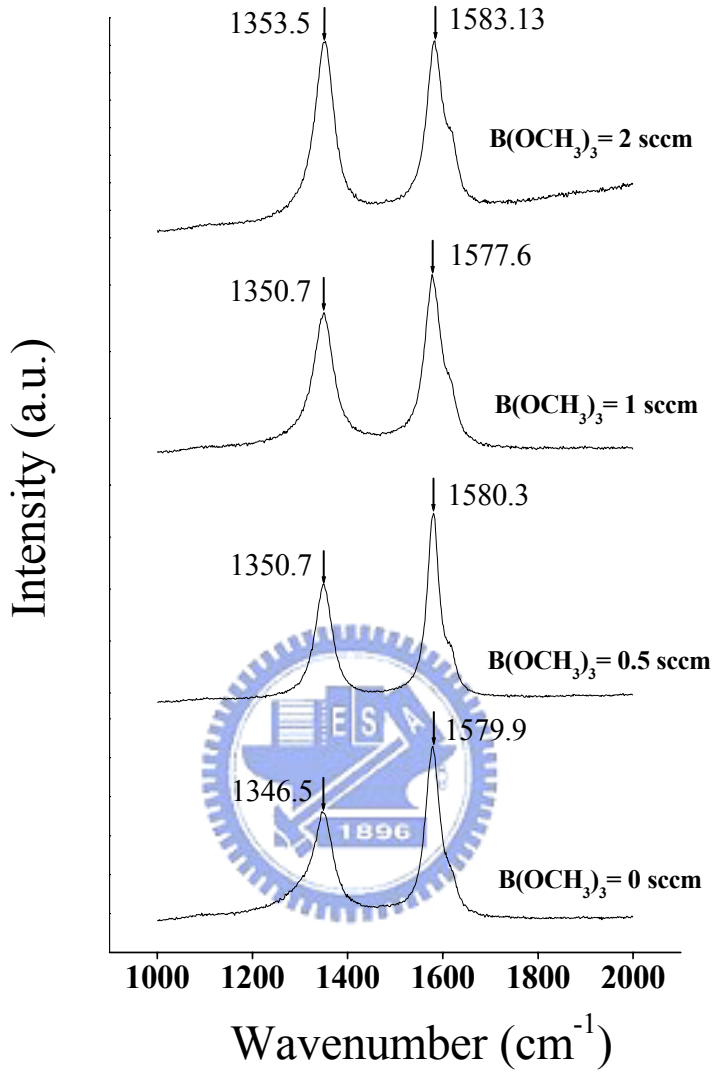

Fig 7.7 Raman spectrum of undoped and various concentrations of boron-doped CNTs

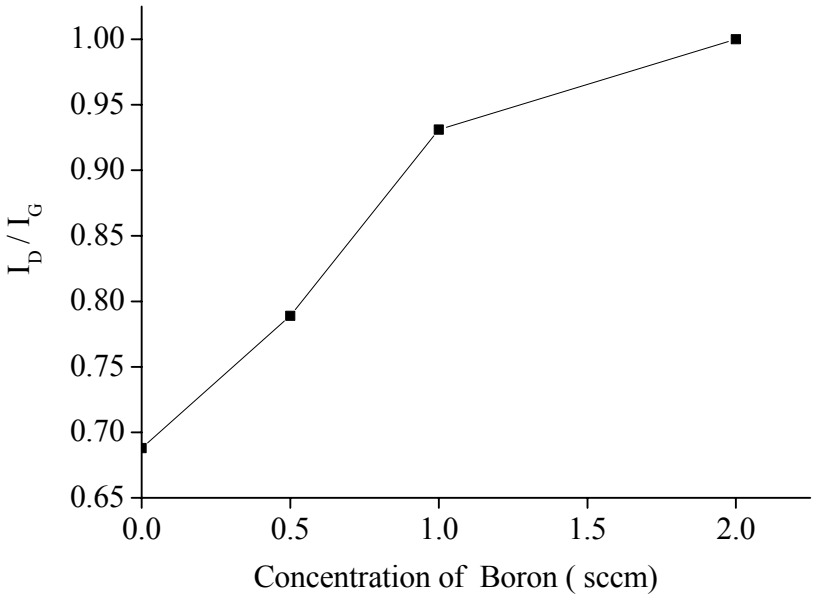

Fig. 7.8 I_D/I_G ratio of undoped and various concentrations of boron-doped CNTs

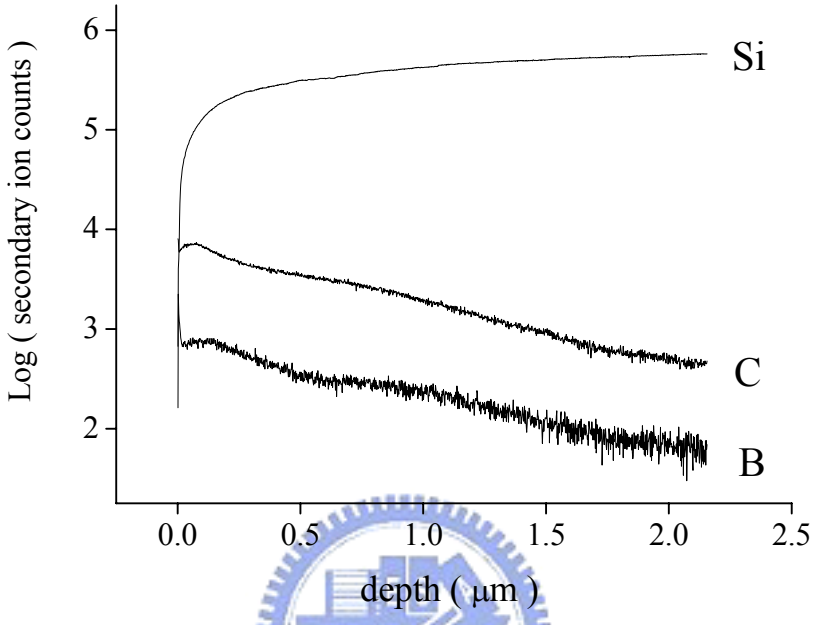

Fig. 7.9 A SIMS depth profile of boron.

(V) I-V measurement

The boron-doped CNT field emission tests are the same statement in the previous chapter 6. Fig. 7.10 presents the current density vs electric field plots for undoped and boron-doped CNTs arrays as well as undoped CNTs film which is without patterns. Obviously, the emitted current density for undoped CNTs arrays (350 mA/cm^2 at 2.2 V/ μm) is much higher than for undoped CNTs films (3.2 mA/cm^2 at 2.2 V/ μm). This is a result at the screening effect [14-15] provoked by the proximity of neighboring CNTs. Besides, boron-doping also improves the field emission characteristics of CNT arrays by 30% increase in the emitted current density (from 350 to 470 mA/cm^2 at 2.2 V/μm). This result reveals that electron conduction band in graphite structure is improved and the emission of electrons is enhanced when p-type dopants are added. Solid state physics indicates that doping p-type dopants will instigate an energy band modification in the materials by generating an acceptor level that provides more electron holes for the materials. Besides, the structure defects on boron-doped CNTs maybe behave as emitting sites for electrons. The respective Fowler-Nordheim (FN) plot (ln (I/V^2) vs. 1/V) are shown in Fig.7.11. Plotting ln (I/V^2) vs. 1/V results in a straight line for applied voltage higher than 700 V, implying the field emission characteristics of CNTs. We further estimate the field enhancement factor β from the constant F-N slope on the assumption of ϕ = 5 eV for CNTs.

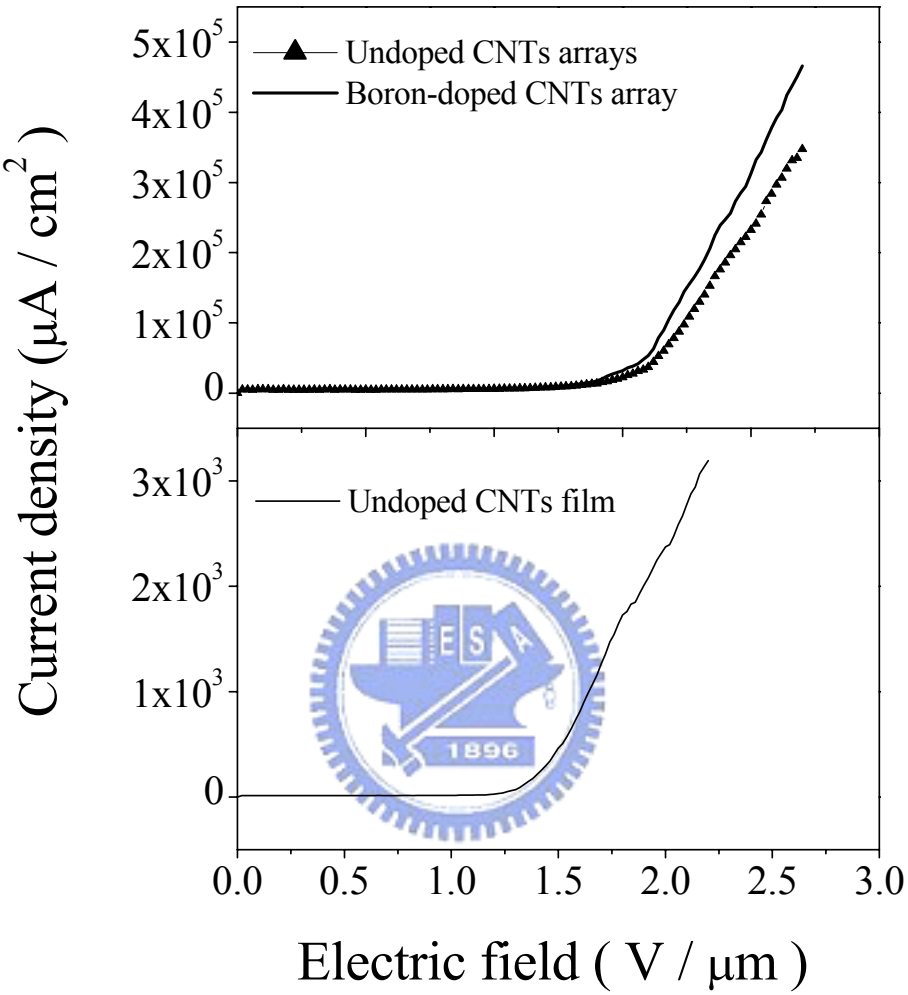

Fig. 7.10 Current density (J)- electric field (E) curve of undoped CNTs films, undoped and boron-doped CNTs arrays.

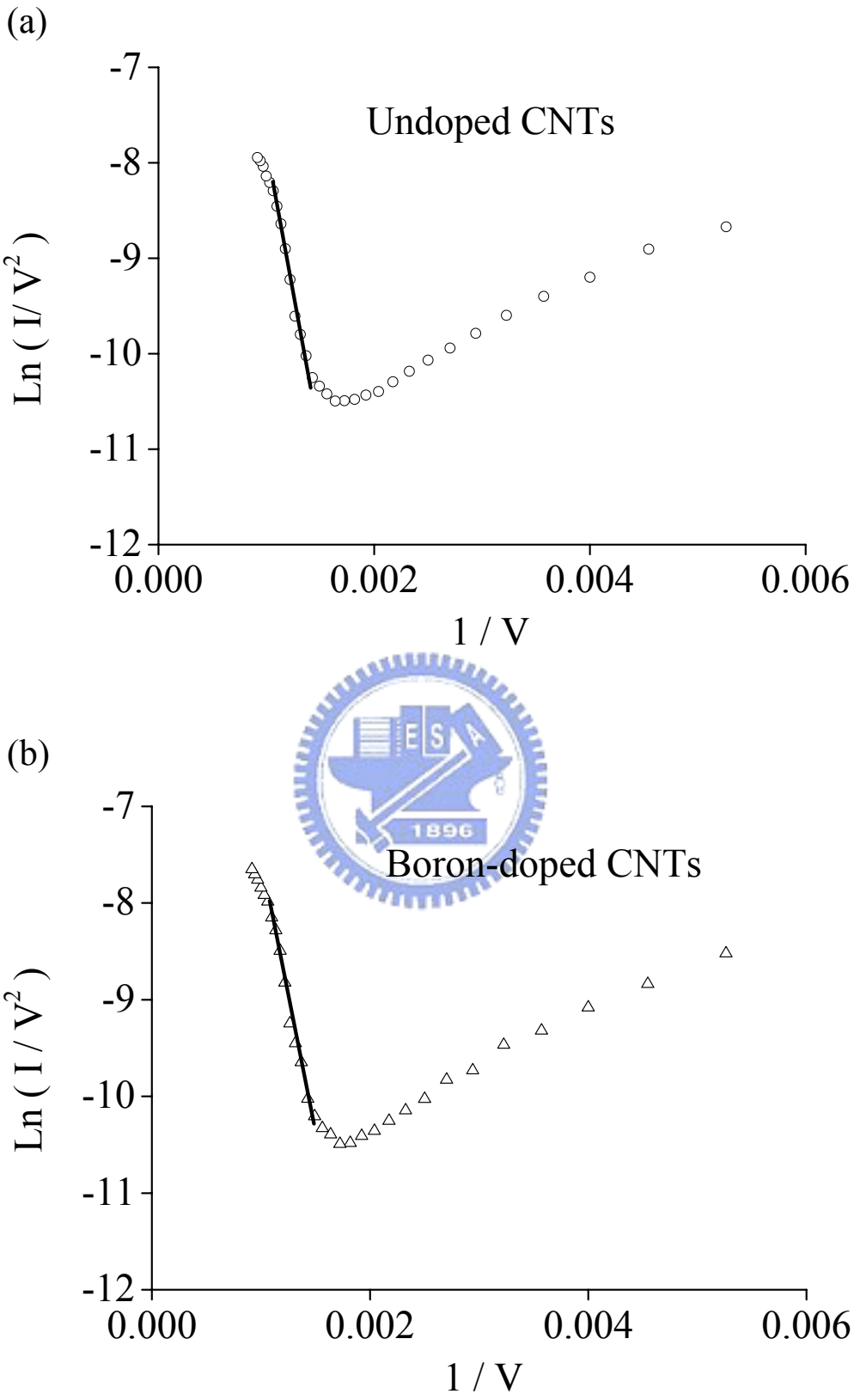

Fig. 7.11 F-N plot of (a) undoped and (b) boron-doped CNTs arrays

Field enhancement factor β for undoped and boron-doped CNTs are approximately 1200 and 1500, respectively. This enhancement is most probably due to the smaller diameter of boron-doped CNTs.

(VI) Resistivity measurement

The resistivity of CNT films is measured by four-point probe (Napson, model RT-7). Measuring condition is under atmosphere and room temperature (RT). From Fig. 7.12, it is obvious that the resistivity of CNT films decreases with increasing boron concentration. Due to the lack of heating apparatus, the measured resistivity is obtained under RT condition. Many studies have pointed out that the resistivity of CNT will decrease with increasing temperature [16-18]. Boron-doped CNT films as compared to pure ones have a reduced resistivity with 40 % drop at RT. Strong effects of the doping boron on the electrical transport behavior of CNT films are expected in the low-temperature range, where charge carrier generation from dopant levels will dominate the temperature dependence of electrical transport [16]. The possibility of improve the electrical transport of CNTs could lead to new strategy of industry application.

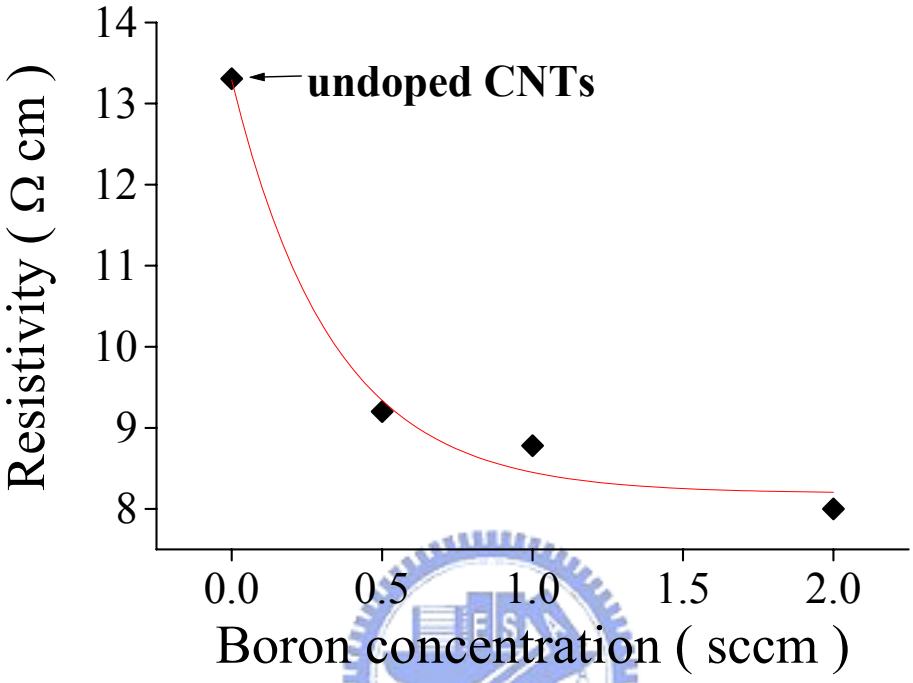

Fig. 7.12 Electrical resistivities of carbon nanotubes film with various boron concentration under room temperature.

7.4. Conclusion

In this chapter, we synthesized boron-doped CNTs by using trimethlborate $B(OCH_3)_3$ as doping source. Experimental results are summarized as follows.

1. Undoped CNTs possess higher growth rate than boron-doped ones because of the existence of oxygen in the doping source.
2. Due to the overgrowing of CNTs grown on catalyst substrate, CNTs grow not only on the Fe substrate but also on the backside, which is catalyst- free substrate.
3. The alignment of CNTs is attributed to crowing effect (Van der Walls effect) not the plasma-induced effect.
4. As used Fe catalyst, the coiled CNTs are found due to the defect-based structure growing model.
5. The intercalation of boron is thought to act as dopants in graphite, in between the graphitic shells leading to an internal strain in the interlayer distances. This internal strain would result in expansion and influence the C-C bonding in graphite structure, leading to defects on CNTs.
6. The nanostructure of bamboo-like shape becomes indistinct with increasing the concentration of boron.
7. The I_D/Ig ratio increases with increasing concentration of boron, implying the decrease of graphitization in boron-doped CNTs.

8. When p-type dopants are added, electron conduction band in graphite structure is improved and the emission of electrons is enhanced. Besides, the structure defects on boron-doped CNTs maybe behave as emitting sites for electrons.

9. Doping boron clearly enhances not only the field enhancement factor β but also emission current density by 30%. In addition, doping effect dominates the electrical transport of CNT films with decreasing the resistivity.

7.5 Reference

1. Ph. Redlich, J. Loeffler, P.M. Ajayan, J. Bill, F. Aldinger, M. Ruhle, Chem. Phys. Lett. V.260, 465 (1996).

2. C.L. Tsai, C.F. Chen and C.L.Lin. J.Appl.Phys.V.90, 4847 (2001).

3. Vladimir I. Merkulov, Anatoli V. Melechko, Michael A. Guillorn, Douglas H. Lowndes, and Michael L. Simpson. Appl. Phys. Lett. 79, 2970 (2001).

4. S. Ihara, S. Itoh, J. Kitakami, Phys. Rev. B 48, 5643, (1993).

5. L.P. Biro, S.D. Lazarescu, P.A. Thiry, et al., Europhys. Lett. 50, 494, (2000).

6. The name Haeckelites is chosen for their architectures, because they resemble (locally) the radiolaria drawings of Ernst Haeckel, in Report on the Scientific Results of the Voyage of the H.M.S. Challenger during the Years 1873–1876, Zoology Vol. 18 (Her Majesty's Stationery Office, London, 1887), Pts. 1–2; E. Haeckel, in Art Forms in Nature (Prestel-Verlag, Munich, 1998).

7. H. Terrones, M. Terrones, E. Hernandez, N. Grobert, J-C. Charlier, . P.M. Ajayan, Phys. Rev. Lett. 84, 1716, (2000).

8. C.F.Chen, T.M.Hang and H.C.Chen. J. Appl. Phys. 74, 4483 (1993).

9. Wang, Xianbao; Hu, Wenping; Liu, Yunqi; Long, Chenfeng; Xu, Yu; Zhou, Shuqin; Zhu, Daoben; Dai, Liming. Carbon. V.39, 1533 (2001).

10. Lee, Cheol Jin; Lyu, Seung Chul; Kim, Hyoun-Woo; Lee, Jin Ho; Cho, Kyoung Ik.

Chem. Phys. Lett. V.359,115 (2002).

11. Li, De-Chang; Dai, Liming; Huang, Shaoming; Mau, Albert W.H.; Wang, Zhong L. Chem. Phys. Lett. V.316,349 (2000).

12. Nemanich, R.J., Solin, S.A., Phys. Rev. B. 20, 392, (1979).

13. Tuinstra, F., Koeing, J.L., J.Chem. Phys. 53, 1126, (1970).

14. P.G.Collins and A.Zettl. Phys. Rev. B V.55, 9391 (1997).

15. O.Groning,O.M.Kuttle, C.Emmenegger, P.Groning, and L.Shlapbach. J.Vac. Sci. Technol. B. V.18, 665 (2000).

16. Bingqing Wei, Ralph Spolenak, Philipp Kohler-Redlich, Manfred Rühle, and Eduard Arzt. Appl. Phys. Lett. 74, 3149 (1999).

17. S. N. Song, X. K. Wang, R. P. H. Chang, and J. B. Ketterson. Phys. Rev. Lett. 72, 697 (1994).

18. Xu, C.L.; Wei, B.Q.; Ma, R.Z.; Liang, J.; Ma, X.K.; Wu, D.H. Carbon. 37, 855, (1999).